

InAs/GaAs *p*-type quantum dot infrared photodetector with higher efficiency

Yan-Feng Lao,¹ Seyoum Wolde,¹ A. G. Unil Perera,^{1,a)} Y. H. Zhang,² T. M. Wang,² H. C. Liu,² J. O. Kim,³ Ted Schuler-Sandy,³ Zhao-Bing Tian,³ and S. S. Krishna³

¹Department of Physics and Astronomy, Georgia State University, Atlanta, Georgia 30303, USA

²Key Laboratory of Artificial Structures and Quantum Control, Department of Physics and Astronomy, Shanghai Jiao Tong University, Shanghai 200240, China

³Center for High Technology Materials, Department of Electrical and Computer Engineering, University of New Mexico, Albuquerque, New Mexico 87106, USA

(Received 23 October 2013; accepted 12 November 2013; published online 13 December 2013)

An InAs/GaAs quantum dot infrared photodetector (QDIP) based on *p*-type valence-band intersublevel hole transitions as opposed to conventional electron transitions is reported. Two response bands observed at 1.5–3 and 3–10 μm are due to transitions from the heavy-hole to spin-orbit split-off QD level and from the heavy-hole to heavy-hole level, respectively. Without employing optimized structures (e.g., the dark current blocking layer), the demonstrated QDIP displays promising characteristics, including a specific detectivity of $1.8 \times 10^9 \text{ cm} \cdot \text{Hz}^{1/2}/\text{W}$ and a quantum efficiency of 17%, which is about 5% higher than that of present *n*-type QDIPs. This study shows the promise of utilizing hole transitions for developing QDIPs. © 2013 AIP Publishing LLC. [<http://dx.doi.org/10.1063/1.4846555>]

In the past decade, the quantum dot infrared photodetector (QDIP), one of the important emerging devices in the field of infrared (IR) technology, has received considerable attention, owing to the advantage of three-dimensional confinement of carriers. The three-dimensional confinement promises to offer normal incidence detection, and improved characteristics, such as low dark current and increased photo-carrier lifetime because of the phonon bottleneck.¹ Significant progress in the past has been achieved using quantum dots (QDs)² and dots-in-a-well (DWELL)³ designs, based on *n*-type electrons. So far, little attention has been paid to *p*-type QDIP. In this letter, we report a *p*-type QDIP operating through optical transitions between different sets of valence-band (VB) QD levels, as opposite to electron transitions between conduction band (CB) QD levels.

Despite the promising characteristics, a major challenge associated with QDIPs is the low quantum efficiency (QE).⁴ For example, the typical QE was obtained to be about 2%.^{4,5} Optimization to 12% can be achieved by utilizing bound-to-bound transitions in a GaAs-based *n*-type DWELL structure,³ which, however, is still less than the QE of HgCdTe and type-II superlattice detectors.⁴ By growing InAs QDs on InP substrate and using the bound-to-bound transition DWELL structure, further improvement to as high as 35% was reported, with the response up to 5 μm .⁶ The relatively low QE of QDIPs results in part from the large fluctuation of the dot size in the Stranski-Krastanov growth mode. This, along with the low QD density as compared to the density of dopants in quantum-well infrared photodetectors (QWIPs),⁷ give rise to the lower absorption efficiency than expected. Although alternative growth methods such as sub-monolayer epitaxy come with the advantage of higher dot density (e.g., $\sim 5 \times 10^{11} \text{ cm}^{-2}$),⁸ designing optimized structures to further improve QE is yet to be demonstrated. Such designs may include a change of operating carrier type from majority electrons to holes, which offers a few unique characteristics,

such as optical transitions associated with three valence bands and higher effective mass of the holes. The former leads to a broad response allowing for convenient tailoring of the spectral response. The latter features increased density of states and thus enhanced absorption, as a great number of holes are allowed in QDs. Also, higher effective mass of holes means the lower dark current compared to conduction through electrons.⁹

Among a variety of photodetectors being investigated, devices based on *p*-type doping^{10,11} are not studied as widely as the *n*-type counterpart. Room-temperature operation by utilizing *p*-type inter-valence-band transitions was recently demonstrated using bulk heterojunctions.^{12–14} Aside from the high-temperature operation, inter-valence-band transitions typically yield a broad-band absorption and detection spanning from 1 μm up to beyond 10 μm .^{14,15} This allows for a convenient tuning of the spectral response by adjusting the heterojunction band offset. However, an intrinsic drawback of using bulk semiconductors is the fast carrier relaxation time, which is, for example, about 0.1 ps for $1 \times 10^{19} \text{ cm}^{-3}$ *p*-type doped GaAs. In contrast, quantum structures such as dots or dots-in-well are demonstrated to have longer lifetime of photocarriers (up to nanoseconds).¹⁶ As such, an integration of the QD structure and *p*-type hole transitions could offer an alternative route to develop high performance QDIPs.

A schematic structure of the *p*-type QDIP grown by molecular beam epitaxy is shown in Fig. 1(a). The absorbing region consists of 10 periods of InAs QDs, between which is an 80-nm thick undoped GaAs barrier. The pyramidal shape QDs have the height and base dimensions of ~ 5 and $\sim 20 - 25$ nm, respectively. The dot density is about $5 \times 10^{10} \text{ cm}^{-2}$. Free holes are introduced by a δ -doping technique. A sheet density of $5 \times 10^{11} \text{ cm}^{-2}$ *p*-type dopants is placed above the QDs, with a 15-nm thick spacer (GaAs) in-between them, which gives about 10 holes per dot.¹⁷ The detectors were processed by wet etching to produce square mesas and depositing metal ohmic contacts onto the top and bottom contact layers. A top ring contact with a window

^{a)}uperera@gsu.edu

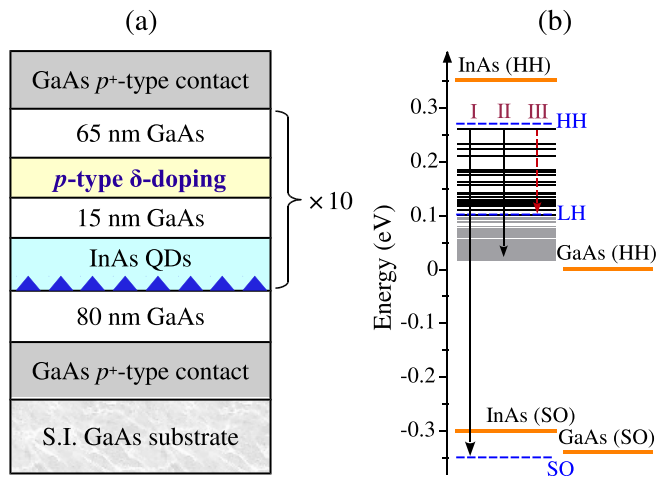


FIG. 1. (a) Schematic of the p -type QDIP structure. Free holes are introduced into QDs by δ -doping above the QD layer. (b) Computed valence band structure of the QDs, where solid lines represent for hole states obtained by using an $8 \times 8 \mathbf{k} \cdot \mathbf{p}$ model.¹⁸ The thick lines are the band edges. The dashed lines are the hole ground states of a QW, which has the same thickness as the QD height. The QW states were obtained using an effective-mass method,²⁰ with the potential confinement adopted from that of the QD in the growth direction through the dot center.^{18,23} The states beyond the LH level become denser due to the larger hole effective mass and also to the LH confinement potential, which leads to a quasicontinuum of tenuously bound states.²² Three transitions (I, II, and III) indicated contribute to the response as observed experimentally, where the transition III only observed at higher biases has the much weaker contribution compared to the other two.

opened in the center was used to allow for front-side illumination. Spectral response was measured on devices with the dimension of $400 \times 400 \mu\text{m}^2$ by using a Perkin-Elmer system 2000 Fourier transform infrared spectrometer. A bolometer with known sensitivity is used for background measurements and calibration of the responsivity.

The hole states in QDs were calculated as shown in Fig. 1(b), by using an $8 \times 8 \mathbf{k} \cdot \mathbf{p}$ model described in Ref. 18. In contrast to only one electron state in the CB, many hole states are allowed in the dots. From numerical computation point of view, this means a massive number of eigenvalues to be solved simultaneously from the eight-band Hamiltonian, which becomes even difficult in the higher hole energy range where dense states¹⁹ are included. To facilitate the computation, the spin-orbit split-off (SO) states were obtained by treating the QD as a quantum well (QW) and using an effective-mass method.²⁰ The much wider in-plane dimension of the dots than the height partially validates such a treatment. The comparison of QD and QW states for the heavy-hole (HH) level, as shown in Fig. 1(b), indicates that the obtained ground states from two approaches are close to each other. We use the QW SO state to represent for the QD SO hole and interpret the spectral response, which should be acceptable for analysis on distinguishing respective contributions of VB hole transitions to the response.

The computed electronic structure of QDs is used to interpret the spectral response of p -QDIP, as shown in Fig. 2(a), displaying two primary response bands at 1.5–3 and 3–10 μm . The overall spectral profile is analogy with that of the p -type GaAs heterojunction detector¹⁴ [Fig. 2(b)]. However, the responsivity of p -QDIP is about 10–20 times higher than that of the heterojunction detector, as shown in Figs. 2(b) and 2(c), despite that QDIP contains a much

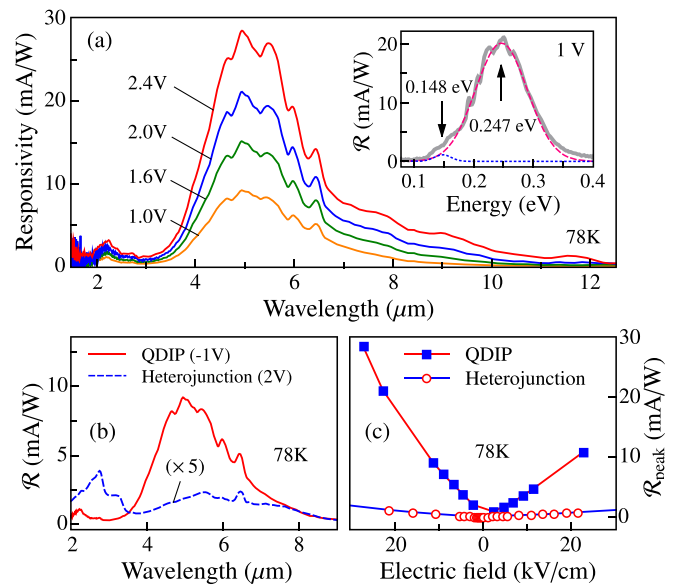


FIG. 2. (a) Spectral response (\mathcal{R}) of the p -type QDIP at 78 K. Two response bands at 1.5–3 and 3–10 μm originate from hole transitions between the SO-HH and HH-HH QD levels, respectively. Inset: Gaussian fits to the spectral response show a lower-energy response peak at 0.148 eV due to the LH-HH transition. (b) Comparison between the response of the p -type QDIP and heterojunction detector.¹⁴ The bias voltages are selected such that they lead to nearly the same electric field. The heterojunction detector consists of 30 periods of p -type GaAs ($3 \times 10^{18} \text{ cm}^{-3}$, 18.8 nm) and $\text{Al}_{0.28}\text{Ga}_{0.72}\text{As}$ (60 nm). Its spectral response was reported elsewhere.¹⁴ (c) The variation of peak responsivity with the electric field. The responsivity of p -QDIP is about 10–20 times higher than that of the heterojunction detector.¹⁴

thinner absorbing region than the heterojunction. This characteristic indicates that the origin of response should be dominantly due to the QDs but not the p -type GaAs contact layers [Fig. 1(a)], benefiting from the longer hole lifetime of QDs. The small spacing between hole states ($<30 \text{ meV}$) leads to varying response with the photon energy in accordance with the band structure of InAs/GaAs. For example, the two response bands lie above and below the SO splitting energy of InAs (0.39 eV or 3.2 μm in wavelength).²¹ The experimental short-wavelength response peak at 0.552 eV corresponds to the hole transition from the HH ground state to the SO state [0.609 eV by calculation as indicated by transition I of Fig. 1(b)], while the long-wavelength peak at 0.247 eV [also see inset of Fig. 2(a)] corresponds to the hole transition from the HH ground state to the state near the GaAs barrier [transition II, calculated as 0.260 eV]. In view of assumed ideal pyramidal shape in the calculations, the agreement between experiment and computed electronic structure is reasonably well.

The hole transition which contributes to the primary response peak at 0.247 eV may end up to quasibound states. It can be seen from Fig. 1(b) that hole states becomes denser¹⁹ at the higher energy portion of the HH confinement potential, due in part to the larger hole effective mass and to the light-hole (LH) confinement potential, which leads to a continuum of tenuously bound states.²² This characteristic is consistent with the broad nature of the response peak with $\Delta\lambda/\lambda = 0.42$, where λ and $\Delta\lambda$ are 5.2 μm and 2.2 μm , respectively. However, the HH bound-to-HH quasibound transition may dominate over the HH bound-to-LH continuum transition, as the bound-to-quasibound transition has the higher

absorption than the bound-to-continuum transition.³ Compared to the HH to HH response, the short-wavelength response contributed by the HH to SO transition is not as strong as in the heterojunction case, as shown in Fig. 2(b). A possible cause is the impact of strain on the local band edges,²³ leading to a much shallower SO confinement potential than the HH band and giving rise to continuum SO states. Additionally, scattering events are required to transfer holes in the SO states to the HH states of the barrier to facilitate transport, which somewhat reduces the escape efficiency.

Typical QDIPs display bias-dependent multiple wavelength responses as a result of the change between bound-to-bound and bound-to-continuum transitions. Such an effect is less pronounced in the present *p*-type detector compared to *n*-type QDIP.²⁴ It was observed that a long-wavelength response tail rises at higher bias as shown in Fig. 2(a), the Gaussian fit of which [inset of Fig. 2(a)] gives its peak at 0.148 eV. In view of its width ($\Delta\lambda/\lambda = 0.23$, where λ and $\Delta\lambda$ are 8.3 μm and 1.9 μm , respectively), this response originates from the HH bound-to-LH bound transition as indicated by transition III of Fig. 1(b) (0.160 eV by calculation).

The dark current-voltage characteristic of the *p*-QDIP is shown in Fig. 3(a), and used, along with the experimentally measured noise current (i_n), to obtain the noise gain (g) through the expression: $g = i_n^2/4eI_d$, where I_d is the dark current. Figure 3(b) plots the noise gain as a function of bias. Assuming that the photoconductive gain equals the noise gain,^{2,6} the value of QE can be calculated from the relationship between the responsivity (\mathcal{R}) and gain: $\text{QE} = \mathcal{R} \times h\nu/eg$, where $h\nu$ is the photon energy. As shown in Fig. 3(c), QE reaches the maximum of 17% at -0.6 V. The specific detectivity is given by $D^* = \mathcal{R}\sqrt{A \times \Delta f}/i_n$, where A is the device area and Δf is the bandwidth. The detectivity at 78 K for the response peak at 5 μm as a function of bias is shown in Fig. 4, with a maximum value of $1.8 \times 10^9 \text{ cm} \cdot \text{Hz}^{1/2}/\text{W}$ at -0.4 V.

It was reported³ that the bias at which the maximum detectivity is obtained progressively varies with the transition type. The optimum operating bias of the bound-to-continuum transition is close to 0 V.³ A recently demonstrated *p*-type

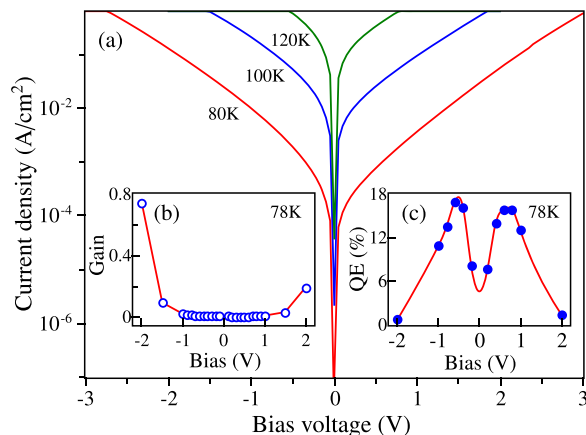


FIG. 3. (a) Dark current density of the *p*-type QDIP at different temperatures. (b) and (c) (shown as insets) are the noise gain and QE, respectively. The noise gain is calculated by using experimentally measured noise current and dark current. QE is obtained by assuming that the photoconductive gain equals the noise gain.^{2,6}

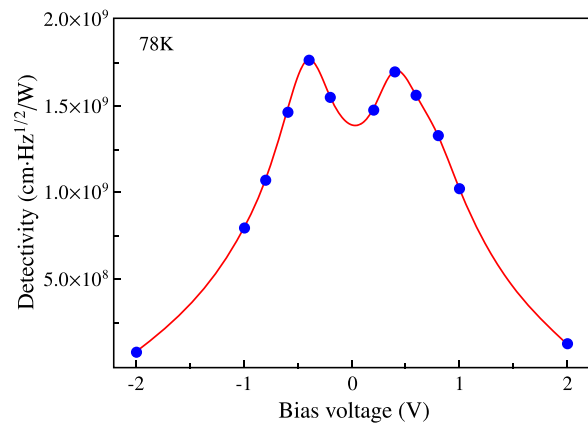


FIG. 4. The specific detectivity of the *p*-type QDIP for the response peak at 5 μm , plotted as a function of the bias.

Ge/Si(001) QDIP¹⁷ based on the bound-to-continuum transition also confirmed this operation. For the InAs/GaAs *p*-QDIP reported here, the bias-dependent detectivity as shown in Fig. 4 indicates the bound-to-quasibound transition as the primary transition contributing to the response, in agreement with the prior analysis based on computed electronic structure [Fig. 1(b)].

It should be noted that the demonstrated *p*-QDIP does not employ a dark current blocking layer [see Fig. 1(a)]. This causes the dark current more than three order of magnitudes higher than that of *n*-QDIPs typically using a blocking layer.²⁵ Although the current blocking layer also reduces the responsivity, the noise is suppressed more effectively, leading to increased signal to noise ratio and the detectivity.²⁵ On the basis of the present structure, further improvement on the QE is possible through optimizing the transition type and enhancing the absorption. Barve *et al.*³ reported the QE values for the bound-to-continuum, bound-to-quasibound, and bound-to-bound transitions, the maximums of which are $\sim 2\%$, 6% , and 12% , respectively. It is therefore expecting an increase in the QE of the *p*-QDIP by operating based on the bound-to-bound hole transitions. The enhancement of absorption could be attained by optimizing the QDs, such as the number, density, and uniformity of the dot layers, and also by employing a resonant cavity.²⁶

A major concern regarding the *p*-QDIP could be the relatively lower mobility of holes, which causes limitation on the speed performance as compared to operation through electrons. However, the structure shown in Fig. 1(a) may not be expected to display significant degradation in the speed performance, owing to the use of undoped materials (except for the δ -doping regions). The mobility is mostly determined by the GaAs barrier as the dots are much thinner. The hole mobility (77 K) of *p*-type GaAs at $p = 10^{18} \text{ cm}^{-3}$ is $900 \text{ cm}^2/\text{V} \cdot \text{s}$, and increases to about $10^4 \text{ cm}^2/\text{V} \cdot \text{s}$ for undoped GaAs.²⁷

To conclude, we have demonstrated the promise of *p*-type hole transitions for QDIPs, with a higher QE of 17% being achieved as compared to previously reported *n*-type QDIPs grown on GaAs substrate.³ Two response bands at 1.5–3 and 3–10 μm were confirmed as being due to hole transitions from the HH to SO level and from the HH to HH level, respectively. The broad response ($\Delta\lambda/\lambda = 0.42$) and

the behavior of the bias-dependent detectivity indicate that the response originates from the bound-to-quasibound transition, agreeing with the computed electronic structure of the QDs. Despite the absence of current blocking layers, a specific detectivity of $1.8 \times 10^9 \text{ cm} \cdot \text{Hz}^{1/2}/W$ was obtained for the response peak at 78 K and at $5 \mu\text{m}$.

This work was supported in part by the U.S. National Science Foundation under Grant No. ECCS-1232184. The Shanghai group acknowledges supports from the National Major Basic Research Projects (2011CB925603), the 863 Program of China (2011AA010205), the Natural Science Foundation of China (91221201, 61234005, and 11074167). Professor H. C. Liu supported this work in all aspects, including carrying out the device processing, reading, and commenting on the manuscript, until his death in October 2013.

- ¹V. Ryzhii, *Semicond. Sci. Technol.* **11**, 759 (1996).
- ²G. Ariyawansa, A. G. U. Perera, G. Huang, and P. Bhattacharya, *Appl. Phys. Lett.* **94**, 131109 (2009).
- ³A. V. Barve, T. Rotter, Y. Sharma, S. J. Lee, S. K. Noh, and S. Krishna, *Appl. Phys. Lett.* **97**, 061105 (2010).
- ⁴A. Rogalski, J. Antoszewski, and L. Faraone, *J. Appl. Phys.* **105**, 091101 (2009).
- ⁵H. S. Ling, S. Y. Wang, C. P. Lee, and M. C. Lo, *Appl. Phys. Lett.* **92**, 193506 (2008).
- ⁶H. Lim, S. Tsao, W. Zhang, and M. Razeghi, *Appl. Phys. Lett.* **90**, 131112 (2007).
- ⁷S. D. Gunapala, S. V. Bandara, C. J. Hill, D. Z. Ting, J. K. Liu, S. B. Rafol, E. R. Blazejewski, J. M. Mumolo, S. A. Keo, S. Krishna, Y. C. Chang, and C. A. Shott, *Proc. SPIE* **6206**, 62060J (2006).
- ⁸J. O. Kim, S. Sengupta, A. V. Barve, Y. D. Sharma, S. Adhikary, S. J. Lee, S. K. Noh, M. S. Allen, J. W. Allen, S. Chakrabarti, and S. Krishna, *Appl. Phys. Lett.* **102**, 011131 (2013).
- ⁹J. R. Hoff, M. Razeghi, and G. J. Brown, *Phys. Rev. B* **54**, 10773 (1996).
- ¹⁰W. Z. Shen, A. G. U. Perera, H. C. Liu, M. Buchanan, and W. J. Schaff, *Appl. Phys. Lett.* **71**, 2677 (1997).
- ¹¹H. C. Liu, F. Szmulowicz, Z. R. Wasilewski, M. Buchanan, and G. J. Brown, *J. Appl. Phys.* **85**, 2972 (1999).
- ¹²A. G. U. Perera, S. G. Matsik, P. V. V. Jayaweera, K. Tennakone, H. C. Liu, M. Buchanan, G. Von Winckel, A. Stintz, and S. Krishna, *Appl. Phys. Lett.* **89**, 131118 (2006).
- ¹³P. V. V. Jayaweera, S. G. Matsik, A. G. U. Perera, H. C. Liu, M. Buchanan, and Z. R. Wasilewski, *Appl. Phys. Lett.* **93**, 021105 (2008).
- ¹⁴Y. F. Lao, P. K. D. D. P. Pitigala, A. G. U. Perera, H. C. Liu, M. Buchanan, Z. R. Wasilewski, K. K. Choi, and P. Wijewarnasuriya, *Appl. Phys. Lett.* **97**, 091104 (2010).
- ¹⁵Y.-F. Lao and A. G. U. Perera, *J. Appl. Phys.* **109**, 103528 (2011).
- ¹⁶M. R. Matthews, R. J. Steed, M. D. Frogley, C. C. Phillips, R. S. Attaluri, and S. Krishna, *Appl. Phys. Lett.* **90**, 103519 (2007).
- ¹⁷A. I. Yakimov, A. A. Bloshkin, V. A. Timofeev, A. I. Nikiforov, and A. V. Dvurechenskii, *Appl. Phys. Lett.* **100**, 053507 (2012).
- ¹⁸H. Jiang and J. Singh, *Phys. Rev. B* **56**, 4696 (1997).
- ¹⁹W. Sheng and J.-P. Leburton, *Appl. Phys. Lett.* **80**, 2755 (2002).
- ²⁰S. L. Chuang, *Physics of Optoelectronic Devices* (Wiley, New York, 1995).
- ²¹I. Vurgaftman, J. R. Meyer, and L. R. Ram-Mohan, *J. Appl. Phys.* **89**, 5815 (2001).
- ²²M. A. Cusack, P. R. Briddon, and M. Jaros, *Phys. Rev. B* **54**, R2300 (1996).
- ²³A. Schliwa, M. Winkelkemper, and D. Bimberg, *Phys. Rev. B* **76**, 205324 (2007).
- ²⁴S. Chakrabarti, X. H. Su, P. Bhattacharya, G. Ariyawansa, and A. G. U. Perera, *IEEE Photon. Technol. Lett.* **17**, 178 (2005).
- ²⁵A. V. Barve and S. Krishna, *Advances in Infrared Photodetectors (Semiconductors and Semimetal Series)*, edited by S. D. Gunapala, D. Rhiger, and C. Jagadish (Elsevier, 2011), vol. 84, Chap. 3, pp. 153–193.
- ²⁶Y.-F. Lao, G. Ariyawansa, and A. G. U. Perera, *J. Appl. Phys.* **110**, 043112 (2011).
- ²⁷M. Sotoodeh, A. H. Khalid, and A. A. Rezazadeh, *J. Appl. Phys.* **87**, 2890 (2000).